THE JOURNAL OF PHYSICAL CHEMISTRY C
A JOURNAL OF THE AMERICAN CHEMICAL SOCIETY

pubs.acs.org/JPCC

Article

Different Dynamic Behavior of Methyl Groups in Crystalline Carbimazole as Revealed by a Multitechnique Experimental and Theoretical Approach

Andrea Scarperi, Elisa Carignani, Francesca Martini, Jan P. Embs, Jan Wąsicki, Giovanni Barcaro, Marco Geppi,* and Aleksandra Pajzderska*

Cite This: *J. Phys. Chem. C* 2023, 127, 5186−5196

Read Online

ACCESS | Metrics & More | Article Recommendations | Supporting Information

ABSTRACT: Dynamic properties of carbimazole (a drug used in hyperthyroidism treatment) were thoroughly investigated by combining solid-state nuclear magnetic resonance spectroscopy and quasielastic neutron scattering with periodic density functional theory (plane-wave DFT) and molecular dynamics simulations. These complementary methods allowed the full description of internal carbimazole motions. Particularly, in crystalline carbimazole, only the reorientations of the two methyl groups were found to be active in the explored timescale. The combination of different techniques allowed the quantitative characterization of the two methyl reorientations, which differ by almost 2 orders of magnitude in the timescale, in agreement with results previously reported in the literature for methyl groups in similar chemical environments. These results could also assume a particular relevance considering the role of methyl groups in determining the biochemical and biological activities of active pharmaceutical ingredients.

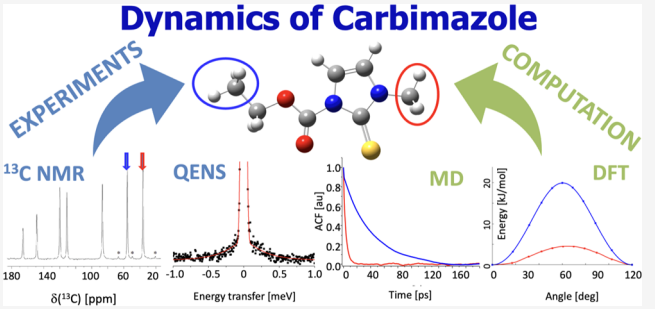

INTRODUCTION

Almost 90% of active pharmaceutical ingredients (APIs) are currently marketed in solid forms (as tablets, powders, or pills) as their oral ingestion is the most comfortable route of drug administration for patients. Most of APIs are in the crystalline state—characterized by long-range ordering of atoms—that has particular physicochemical properties like melting point, solubility, chemical stability, and dissolution rates, which determine the APIs' bioavailability.[1,2] The latter can be associated to molecular arrangement and to intra- and intermolecular forces, which influence the molecular mobility and, in particular, reorientations of molecular groups.[3−5]

In this perspective, both the accurate characterization of the three-dimensional structure and of the molecular dynamics are extremely important. The determination of the solid-state structure of crystalline compounds can be effectively achieved through X-ray diffraction methods, but their combination with solid-state NMR (SSNMR) spectroscopy and DFT methods has proved to be beneficial.[6−9] At the same time, for a detailed characterization of molecular dynamics, requiring the identification of molecular motions and their geometries, as well as the determination of their activation barriers and correlation times, it is important to combine different and complementary experimental and theoretical methods. Among them, SSNMR, quasielastic neutron scattering (QENS), molecular dynamics (MD) simulations, and first-principles calculations are particularly useful.

QENS and SSNMR are the methods of choice to study internal molecular motions across different timescales (from ps to s for NMR and from ps to ns for QENS). Both methods provide information about the correlation times and activation barriers for molecular reorientations and are widely used in the study of pharmaceutical compounds.[10−18] As neutrons are scattered incoherently mainly by hydrogen atoms, QENS is sensitive to self-dynamics of these atoms also giving information about the geometry of selected motions.[19] At the same time, the possibility of exploiting different nuclei and a large variety of nuclear interactions makes SSNMR a versatile tool that allows molecular motions to be identified, localized on the respective molecular fragments, and quantified.[5,20,21]

The combination of these experimental techniques with computational methods can allow a more complex understanding of the dynamic properties in crystalline solids. Classical molecular dynamics (MD) simulations can be performed for relatively large supercells at long simulation timescales as a function of temperature. The timescale of

Received: February 9, 2023
Revised: February 21, 2023
Published: March 2, 2023

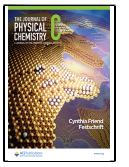

https://doi.org/10.1021/acs.jpcc.3c00904
J. Phys. Chem. C 2023, 127, 5186−5196

molecular motions and their activation barriers probed by MD can be directly compared with SSNMR and QENS results. Also, first-principles approaches can provide information on the dynamic properties via a direct study of the time evolution of the system (via Born−Oppenheimer or Car−Parrinello[22] methods) or, indirectly, via the estimation of the activation barriers of specific internal motions. The latter approach will be used here exploiting the nudged elastic band (NEB) method coordinates[23] at the DFT level of theory to reconstruct the profile of the potential energy surface along specific internal motions.

The present paper is focused on the exploration of molecular dynamics in crystalline carbimazole by combining experimental and computational methods. Carbimazole is an active pharmaceutical ingredient, widely used for the treatment of overactive thyroid (hyperthyroidism) and Grave's disease. Its antithyroid action is attributed to its metabolization to methimazole in the body, which inhibits the first step of thyroid hormone synthesis in thyroglobulin.[24−27] Carbimazole belongs to the class of imidazoles with a methyl group bonded to one nitrogen atom, and with an ethoxycarbonyl chain bonded to a second nitrogen (Figure 1). In our previous paper high-resolution SSNMR methods combined with DFT-GIPAW calculations were applied to refine the crystal structure of carbimazole.[28]

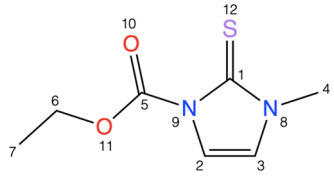

Figure 1. Molecular structure of carbimazole with atom labeling.

The aim of the present paper is to investigate in detail and to get better insight into the molecular motions of carbimazole. Results from QENS and SSNMR methods are compared and interpreted with the precious aid of MD and DFT techniques. Such complementary study allows all of the internal motions to be identified, assigned to specific molecular moieties, and quantified in terms of activation energies and correlation times.

MATERIALS AND METHOD

Sample. Crystalline carbimazole (2,3-dihydro-3-methyl-2-thioxo-1H-imidazole-1-carboxylic acid ethyl ester) was purchased from TCI, (Tokyo, Japan) (CAS RN 22232-54-8) and used as it was.

Quasielastic Neutron Scattering (QENS). QENS measurements of carbimazole were performed on a FOCUS (PSI, SINQ) time-of-flight spectrometer. The powder sample was placed in a hermetically sealed flat aluminum holder (30.0 mm × 40.0 mm) with a sample thickness of 0.3 mm (mass of sample = 1.1 g) to achieve sufficient intensities and avoid multiple scattering. QENS spectra were collected in the Q-range 0.3−1.8 Å^{-1} using a PG002 monochromator, giving an incoming neutron wavelength λ_0 = 5.75 Å and an energy resolution of about 0.08 meV (FWHM). The measurements were performed at 200, 250, and 300 K, and each spectrum was collected approximately for 4 h. Additionally, measurements were performed on an empty holder and a vanadium sample at room temperature to be used in the background and normalization procedures, respectively.

Raw data were treated with the DAVE package,[29] which performs the standard corrections, including background subtraction and self-absorption correction. Then, using the vanadium spectrum as an elastic scattering standard, the intensities were normalized to correct for different detector efficiencies. Finally, the signals from the detectors contaminated by Bragg peaks were ignored and removed from further analysis to focus only on the incoherent quasielastic neutron scattering part. The spectra were fitted using the *STR_FIT* program in Lamp,[30] which enables numerical convolution with the instrumental resolution function $R(Q,\omega)$ determined from a measurement of a vanadium standard sample.

Solid-State Nuclear Magnetic Resonance (SSNMR). SSNMR experiments were recorded on a Bruker Avance Neo spectrometer working at Larmor frequencies of 500.13 and 125.77 MHz for ^{1}H and ^{13}C nuclei, respectively, equipped with a double-resonance cross-polarization magic angle spinning (CP MAS) probehead accommodating rotors with an external diameter of 4 mm. The 90° pulse duration was 2.75 and 3.85 μs for ^{1}H and ^{13}C, respectively. The ^{1}H−^{13}C CP MAS spectrum was recorded using a contact time of 2 ms and accumulating 64 scans. The ^{1}H direct excitation (DE) MAS spectrum was recorded accumulating 8 scans. ^{1}H spin−lattice relaxation times in the laboratory frame (T_1) were measured using an inversion-recovering pulse sequence with variable delays ranging from 1 ms to 25 s. ^{13}C spin−lattice relaxation times in the laboratory frame (T_1) were measured using the Torchia pulse sequence[31] with variable delays ranging from 1 ms to 40 s. All of the ^{13}C experiments were performed under high-power decoupling (HPD) from ^{1}H nuclei during signal acquisition. All of the experiments were carried out at a MAS spinning frequency (ν_{MAS}) of 15 kHz. The relaxation measurements were performed in a temperature range of 286 to 362 K. The temperature calibration was carried out referring to the ^{207}Pb chemical shifts of $Pb(NO_3)_2$, determined using a 50/50 w/w mixture of lead nitrate and adamantane to reduce the sample density and safely reach the spinning frequency of 15 kHz.[32] The relaxation delays were between 25 and 30 s for ^{1}H and between 7 and 26.5 s for ^{13}C depending on the experimental temperature.

DFT Methods. DFT investigation was carried out using an approach analogous to that reported in ref 31. In details, all of the simulations used the Quantum Espresso (QE) suite of programs,[33] employing PAW (plane-augmented waves) pseudopotentials,[34] the PBE-D2 XC-functional,[35,36] and plane waves as basis sets to build Bloch states. The crystal structure of carbimazole was extracted from the experimental data of the JOVDIH01 structure (crystal axes measuring 7.698, 6.650, and 17.388 Å within an orthorhombic cell belonging to the *Pnma* space group)[37] and locally reoptimized. Cutoffs on the wave function and electronic density were set to 60/600 Ry (1 Ry = 313.8 kcal/mol); the first Brillouin cell in the reciprocal space was sampled according to a converged (4 × 4 × 2) mesh of k-points; calculations were performed spin-restricted by applying a Gaussian smearing of the one-particle energy levels of 0.002 Ry. Activations barriers were estimated at zero temperature by applying the NEB (nudged elastic band) method[23] as implemented in QE software.

Molecular Dynamics Simulations. Molecular dynamics (MD) simulations of crystalline carbimazole were performed using DL_POLYClassic.[38] The supercell of dimensions ~40 × 40 × 40 Å^3 containing 160 carbimazole molecules was constructed on the basis of X-ray diffraction data refinement

https://doi.org/10.1021/acs.jpcc.3c00904
J. Phys. Chem. C 2023, 127, 5186−5196

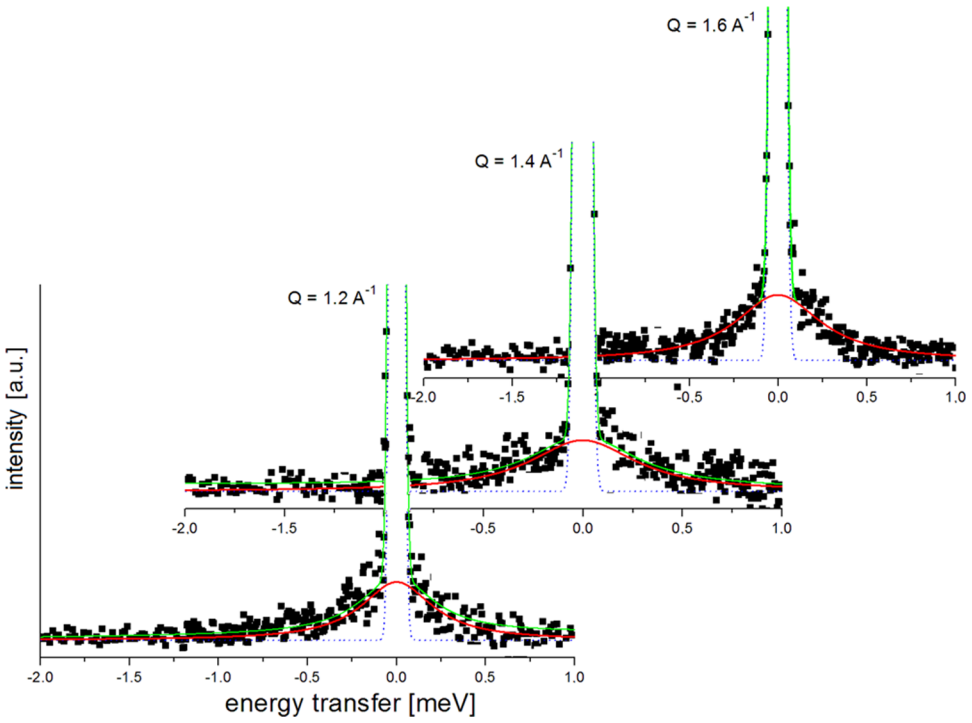

Figure 2. Normalized QENS spectra of carbimazole, recorded on a FOCUS spectrometer at 250 K. The experimental data (black squares) are compared to the fitted model (eq 1, green lines). The individual elastic (blue dotted lines) and the quasielastic (red lines) components are also shown.

in our previous paper.[28] MD simulations were performed at three different temperatures (250, 225, and 200 K) at constant NVT using a Berendsen's thermostat[39] with a relaxation constant of 1 ps. Periodic boundary conditions were applied in all directions, a cutoff distance of 19 Å was applied for the van der Waals forces, and the electrostatic interactions were treated using the Ewald summation method with the same cutoff in real space. The oplsa2005 force field was used. In all cases, a time step of 1 fs was used and the systems were equilibrated during 1 ns. Then, the trajectory was saved every 1 ps for a total simulation time of 10 ns. The analysis of the trajectories was then performed using nMoldyn 3[40] and self-written programs.

RESULTS

Quasielastic Neutron Scattering. A first investigation of molecular mobility in carbimazole was performed by quasielastic neutron scattering measurements, performed using a FOCUS spectrometer with a resolution of ∼0.08 meV (FWHM) and probing motions on the ps timescale. From the structure of the carbimazole molecule, it can be inferred that only the motions of the methyl groups can be potentially detected by this technique.

A quasielastic broadening is clearly visible at 250 K (Figure 2) and 300 K, and QENS spectra were fitted to the model (convoluted with the resolution function $R(Q,\omega)$)

$$S(Q,\omega) = A_0(Q)\cdot\delta(\omega) + (1 - A_0(Q)L(\Gamma,\omega) + B(Q,\omega) \quad (1)$$

where $A_0(Q)$ is the elastic incoherent structure factor (EISF), $L(\Gamma,\omega)$ is a Lorentzian function of full width at half-maximum Γ, and $B(Q,\omega)$ describes the linear background. The above fit permits to determine $A_0(Q)$ and Γ (which is inversely proportional to the correlation time). The former provides information about the geometry of motions, while the latter can be compared with the correlation times obtained from NMR measurements and computational (DFT and MD) analysis.

All of the spectra can be well described by eq 1, i.e., using a single Lorentzian function. Since two methyl groups (carbons 4 and 7) in carbimazole may reorient with different characteristic times, additional fits to two Lorentzian functions, each corresponding to the reorientation of a single methyl group, were performed. However, no improvement was observed and the fit to a single Lorentzian line very well reproduces the quasielastic broadening. This implies that either the reorientation of only one methyl group is visible by QENS or the correlation times of the reorientations of the two methyl groups are so similar that they cannot be separated. These two options will be discussed later.

The width of the Lorentzian line (within the uncertainty limit) does not depend on Q (see Figure S1), directly indicating the local nature of the described motion. So, assuming a reorientational motion of a methyl group about its ternary symmetry axis, consisting in jumps among the three conformations of minimum energy, the corresponding elastic incoherent structure factor can be written as[19]

$$A_0^{CH_3}(Q) = \frac{1}{3}[1 + 2j_0(Qd)] \quad (2)$$

where d is the distance between protons in the CH_3 group. All of the atoms of the molecule contribute in principle to the EISF, nevertheless the contribution from the hydrogen atoms is more than 90% of the total scattering, i.e., the contribution from all other elements (nitrogen, carbon, oxygen, and sulfur) can be neglected. Therefore, the measured elastic incoherent structure factor can be expressed as

https://doi.org/10.1021/acs.jpcc.3c00904
J. Phys. Chem. C 2023, 127, 5186−5196

$$A_0(Q) = (1 - c) + c \cdot A_0^{CH_3}(Q) \quad (3)$$

where c is the fraction of mobile hydrogen atoms in the experimental timescale, i.e., the ratio between the number of the hydrogen atoms in the rotating methyl groups and the total number of hydrogens in the carbimazole molecule.

The EISF extracted from the fit of the QENS spectra using eq 1 is shown in Figure 3 together with the fits to eq 3, carried

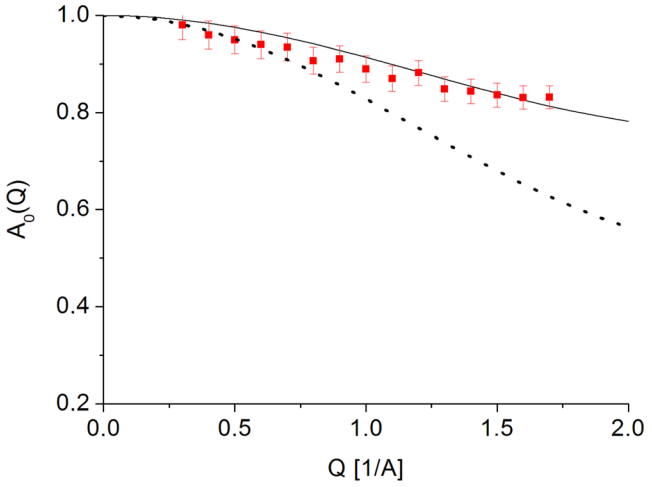

Figure 3. Experimental EISF extracted from QENS data at T = 250 K (red squares). The solid and dotted lines show the theoretical EISF corresponding to the reorientation of one and two methyl groups, respectively (eq 3).

out assuming the reorientation of one (c = 0.3) or two (c = 0.6) methyl groups. The EISF is very well described by the model assuming the reorientation of one methyl group, indicating that only this motion is observed by the QENS experiment. Its correlation time can be calculated from the half-width Γ of QENS spectra, being Γ related to the correlation time τ_c by the expression $\tau_c = 3\hbar/(2\Gamma)$ in a three-site jump model.[19] The extracted correlation times are equal to 5.3 ps (250 K) and 3.6 ps (300 K) and were used to determine the activation energy (5.3 kJ/mol) through the Arrhenius relation.

Solid-State NMR. *Identification of Active Internal Motions.* The ^{13}C CP MAS spectrum of carbimazole recorded at room temperature and at ν_{MAS} = 15 kHz is reported in Figure 4. Similar spectra were already obtained by us at ν_{MAS} = 22 kHz and are reported in ref 28. The ^{13}C CP MAS spectrum shows seven narrow and well-resolved peaks, which are assigned to the seven inequivalent carbon nuclei of carbimazole, as shown in Figure 4.

The ^{13}C and ^{1}H T_1's measured at different temperatures are reported in Table 1. A first observation concerns the order of magnitude of the values obtained for the different carbons: the ^{13}C nuclei belonging to the imidazole ring (C1, C2, C3) and to the carbonyl moiety (C5) exhibit very long spin−lattice relaxation times (>200 s), which could not be measured with a sufficient accuracy and therefore are not reported in Table 1. The two methyl carbons C4 and C7 and the methylene carbon C6, on the other hand, show shorter T_1 values, which could be measured with a satisfactory accuracy and are suitable for a quantitative study of the molecular motions involving these nuclei. All of these carbons exhibit a monoexponential relaxation decay throughout the temperature range experimentally explored: for C4 and C6, T_1's are of the order of tens of seconds, while for C7, it assumes values of the order of hundreds of milliseconds to one second.

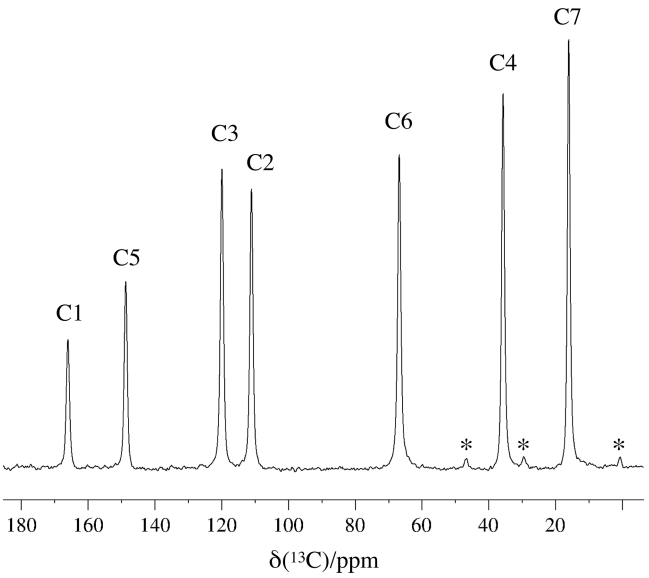

Figure 4. ^{13}C CP MAS spectrum recorded at ν_{MAS} = 15 kHz. Spectral assignment is reported, referred to carbon labeling of Figure 1. Spinning sidebands are marked with asterisks.

Table 1. ^{1}H and ^{13}C T_1 Values Measured at the Indicated Temperatures

T (K)	^{1}H T_1 (s)	^{13}C C4 T_1 (s)	^{13}C C6 T_1 (s)	^{13}C C7 T_1 (s)
286	1.32	14.7	22	0.32
291	1.43			
295	1.55	14.8	26	0.40
299	1.68			
303	1.86	15.4	32	0.47
307	2.00			
312	2.24	15.6	36	0.56
316	2.35			
320	2.53	16.3	41	0.71
324	2.75			
329	3.08	16.5	45	0.83
333	3.22			
337	3.48	16.8	51	1.01
341	3.73			
345	4.04	17.6	59	1.20
350	4.35			
354	4.64			1.36
358	5.08			
362	5.33			1.51

The increasing trends of T_1 values shown by C7, C6, and C4 with increasing temperature clearly indicate that all of the motions mainly responsible for the spin−lattice relaxation of these nuclei belong to the fast motion regime, i.e., their correlation times satisfy the condition $\tau_C < 1/\omega_{0C}$, being ω_{0C} the ^{13}C Larmor frequency.

In particular, the C7 T_1 values are of the order of hundreds of milliseconds at room temperature, i.e., close to the value expected at the T_1 minimum for a methyl carbon,[41−45] suggesting that the correlation time for the reorientation of this methyl group around its symmetry axis is only slightly below $1/\omega_{0C}$.

https://doi.org/10.1021/acs.jpcc.3c00904
J. Phys. Chem. C 2023, 127, 5186−5196

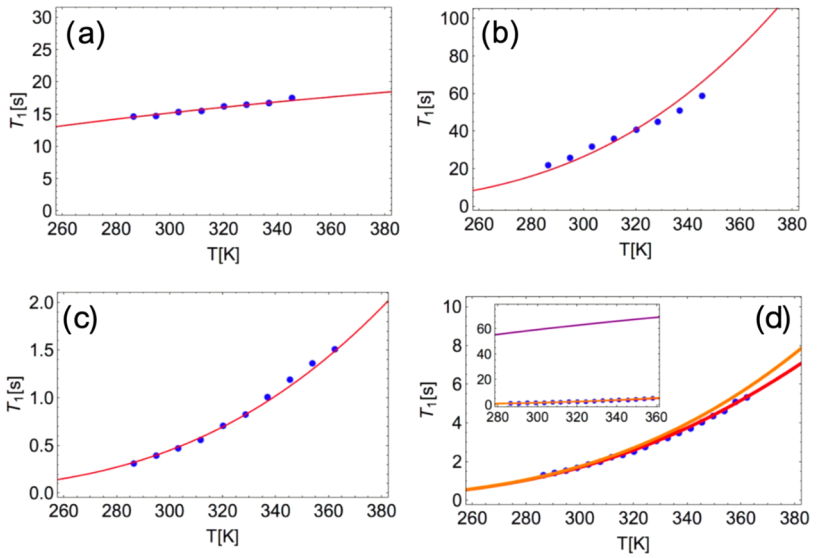

Figure 5. (a–c) ^{13}C spin–lattice relaxation times measured at the Larmor frequency of 125.77 MHz vs temperature: (a) C4, (b) C6, and (c) C7. (d) ^{1}H spin–lattice relaxation times measured at the Larmor frequency of 500.13 MHz vs temperature. Experimental data (blue circles), the results of the global fitting procedure described in the text (red lines), and individual contributions to ^{1}H relaxation arising from the reorientations of the methyl groups 7 and 4 (orange and purple lines, respectively) are reported. The same data extrapolated on a broader T_1 range are shown in the inset of panel (d).

In the case of C6, the combination of T_1 values of tens of seconds and their increasing T_1 trend with increasing temperature allows us to exclude the presence of a reorientation of the ethyl group around the C6–O11 bond. In fact, if such motion was present, C6 T_1 > C7 T_1 would implicate the physically unreasonable case that the correlation time of this motion is shorter than that describing the rotation of the methyl group 7 around its ternary symmetry axis. Instead, it will be shown in the following that the C6 T_1 values are fully compatible with a frozen O–CH_2 group (previously suggested by Delage et al.[46]) and a spin–lattice relaxation of C6 due to the modulation of its coupling with the ^{1}H nuclei of the rotating methyl group 7.

The C4 T_1 values are unusually high for a methyl carbon and they slightly increase with temperature, indicating that the rotation of the methyl group 4 around its symmetry axis is too fast to cause an effective spin–lattice relaxation of C4. This unusual behavior, very different from that of C7, will be further discussed in the following.

^{1}H spin–lattice relaxation trends are effectively described by a single exponential function throughout the investigated temperature range (see Table 1), indicating that spin–diffusion completely averages the different intrinsic ^{1}H spin–lattice relaxation times to a single value. The ^{1}H T_1 values show an increasing trend with increasing temperature, and therefore, the correlation times of the motions mainly responsible for this relaxation are less than the inverse ^{1}H Larmor frequency ($\tau_C < 1/\omega_{0H}$). Considering the previous analysis of carbon relaxation, we can preliminarily identify such motions with those of methyl groups 4 and 7.

Quantitative Characterization of Dynamic Processes. A quantitative analysis of the dynamic processes affecting spin–lattice relaxation was performed through a global fitting of all of the available experimental data curves (^{13}C T_1 of C4, C6, and C7 and ^{1}H T_1) vs temperature, carried out using eqs 4 and 5, derived from the theory of nuclear spin relaxation[42]

$$\frac{1}{T_{1C}} = \frac{n}{20}\left(\frac{\mu_0}{4\pi}\right)^2 \frac{\hbar^2\gamma_H^2\gamma_C^2}{r_{CH}^6}[J(\omega_{0H} - \omega_{0C}) + 3J(\omega_{0C}) + 6J(\omega_{0H} + \omega_{0C})] \quad (4)$$

$$\frac{1}{T_{1H}} = C_H \sum_i a_i[J_i(\omega_{0H}) + 4J_i(2\omega_{0H})] \quad (5)$$

where γ_H and γ_C are the gyromagnetic ratios for ^{1}H and ^{13}C nuclei, respectively, n is the number of hydrogen atoms directly bonded to the relevant carbon atom, r_{CH} is the carbon–hydrogen bonding distance, and C_H is a proportionality constant obtained as the best-fit parameter. In eq 5, the sum runs over all of the motional processes contributing to ^{1}H relaxation (in our case, the reorientation of the two methyl groups 4 and 7), and a_i is the corresponding relative weight. The functions $J(\omega)$ are the spectral densities, expressed in terms of correlation times following the simplest Bloembergen–Purcell–Pound model

$$J(\omega) = \frac{2\tau_c}{1 + \omega^2\tau_c^2} \quad (6)$$

Equation 4 was used with the parameters described above for C7 and C4. For C6, considering the previous observation about the O–CH_2 group being frozen, n = 3 (the number of hydrogen atoms of the methyl group 7) was used, and r_{CH} was taken as the average distance between C6 and H7. For C4, the presence of additional contributions to ^{13}C relaxation arising from the fluctuations of the intermolecular heteronuclear dipolar interactions between carbon C4 and the ^{1}H nuclei of the four closest methyl groups 7 surrounding the methyl group 4 in the crystal unit was also considered. Nonetheless, such contributions revealed very small and were not included in the final model used to fit the data.

The global fitting procedure was applied to obtain more robust and reliable results (e.g., correlation times τ_C and activation energies E_a) with respect to those obtained through

https://doi.org/10.1021/acs.jpcc.3c00904
J. Phys. Chem. C 2023, 127, 5186–5196

separate fits of single curves.[41,42] All of the experimental curves were satisfactorily reproduced considering the model described above, although the methyl reorientations were treated as generic isotropic reorientations (Figure 5). In Figure 5d, the individual contributions to ^{1}H T_1 coming from the reorientations of either the methyl group 4 or 7 are reported: it is clear how the reorientation of the methyl group 7 acts as the relaxation sink at the temperatures and frequency considered, while the reorientation of the methyl group 4 is very fast and its effect on ^{1}H spin−lattice relaxation is small and visible only at temperatures above 310 K. The activation energies and the correlation times obtained are reported in Table 2. By comparing the motions of the two methyl groups, it is interesting to note that the activation energy found by NMR is about 1 order of magnitude lower for the reorientation of the methyl group 4 (2.3 kJ/mol vs 17.3 kJ/mol), for which also the correlation time at 300 K is more than 1 order of magnitude lower (≈1.0 ps vs 35 ps). With respect to the results obtained for the reorientation of the methyl group 4 by QENS, both the correlation time at 300 K (1.0 ps vs 3.6 ps) and the activation energy (2.3 kJ/mol vs 5.3 kJ/mol) found by NMR are significantly lower. For this motion, considering its scarce efficiency to spin−lattice relaxation and the strong correlation between the two best fitting parameters which define it (Arrhenius pre-exponential factor and activation energy), we expect that the results obtained by QENS are more reliable.

Table 2. Activation Energies and Correlation Times Obtained by NMR, DFT, QENS, and MD

	reorientation of methyl 4	reorientation of methyl 7
E_a [kJ mol^{-1}] (NMR)	2.3	17.3
E_a [kJ mol^{-1}] (QENS)	5.3	
E_a [kJ mol^{-1}] (DFT)	4.5	19.9
E_a [kJ mol^{-1}] (MD)	4.8	18.4
log(τ_∞[s]) (NMR)	−12.4	−13.5
log(τ_∞[s]) (QENS)	−12.3	
τ_c [ps] at 300 K (NMR)	1.0	35
τ_c [ps] at 300 K (QENS)	3.6	
τ_c [ps] at 300 K (MD)	3.8	37

The NMR data were also analyzed using a more specific three-site jump model for methyl reorientations:[47,48] the reproduction of the experimental data was equally good, and the same activation energies but Arrhenius pre-exponential factors (and therefore correlations times) differing by a factor of 3 were obtained.

Molecular Dynamics Simulations and DFT Calculations. The motional process identified above by QENS and NMR are related to the reorientation of the methyl groups belonging to the carbimazole molecule. The occurrence of some mobility for the ethoxycarbonyl group could be rejected from NMR data. Nevertheless, to confirm this result, MD simulations were performed also considering this possible motion.

First, the three dihedral angles for the atoms belonging to the ethoxycarbonyl chain were calculated (C2−N9−C5−O11, N9−C5−O11−C6, and C5−O11−C6−C7) along the trajectory. Their time dependence (Figure 6) clearly shows fast oscillations around the equilibrium positions, but no reorientational jumps are observed for all of the molecules in the system. This result is in line with NMR data showing that the reorientation of the ethyl group around the C6−O11 bond is frozen.

The geometry of the possible motion can also be analyzed by the orientational distribution function $P(\Theta)$, calculated as

$$P(\Theta) = \frac{1}{N_{step}} \frac{1}{N_{group}} \sum_{i=1}^{N_{step}} N_i(\Theta, \Theta + d\Theta) \quad (7)$$

where $N_i(\Theta,\Theta + d\Theta)$ is the number of considered groups found with an orientation in the range $(\Theta,\Theta + d\Theta)$ at the ith step. The results are also shown in Figure 6. In all cases, one preferred position is clearly visible and the orientational distribution function $P(\Theta)$ shows a single peak at 180°, confirming a stable planar conformation of the chain and an almost planar (∼30°) conformation of the chain with respect to the plane of the imidazole ring. The mean square displacement (MSD) was also calculated for individual atoms in the carbimazole molecule during the full trajectory, and it remains constant along the time of simulations. This means, as one could expect, that carbimazole molecules do not diffuse in the crystal: nevertheless, the equilibrium values of MSD for different atoms are different (Table S1). The MSDs of C6 and C7 are higher (∼0.22 to 0.26 Å^2) than those of C5 and atoms belonging to the imidazole ring (0.16 Å^2). Such results suggest the occurrence of librations of the ethyl chain around the C6−O11 bond and are consistent with NMR data.

Furthermore, the dynamics of both the methyl groups was analyzed by following the behavior of their C−H bond vectors.

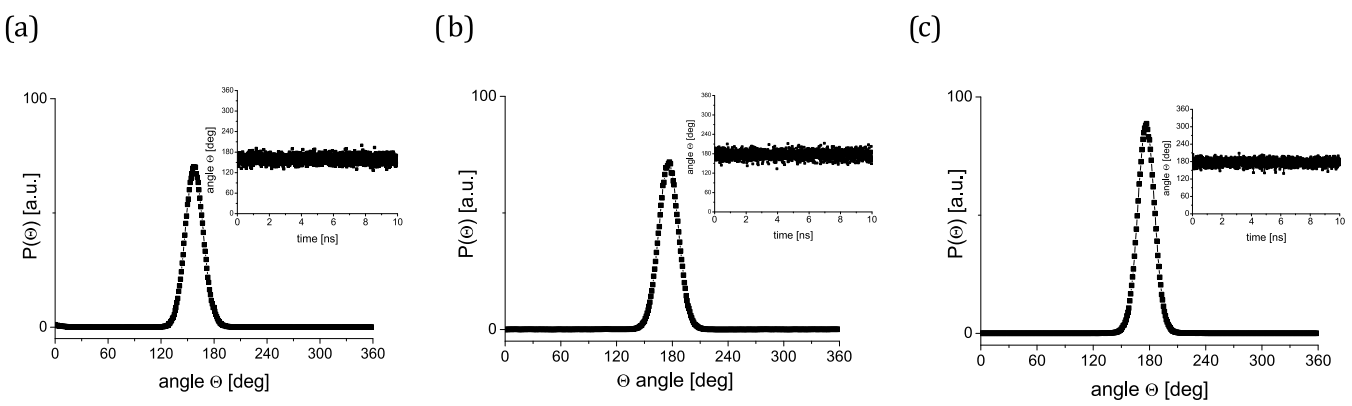

Figure 6. Angular distribution function P(Θ) calculated for the dihedral angles: (a) C2−N9−C5−O11, (b) N9−C5−O11−C6, (c) C5−O11−C6−C7. The insets display the time dependence along the trajectory of the torsional angles for a randomly selected carbimazole molecule.

https://doi.org/10.1021/acs.jpcc.3c00904
J. Phys. Chem. C 2023, 127, 5186−5196

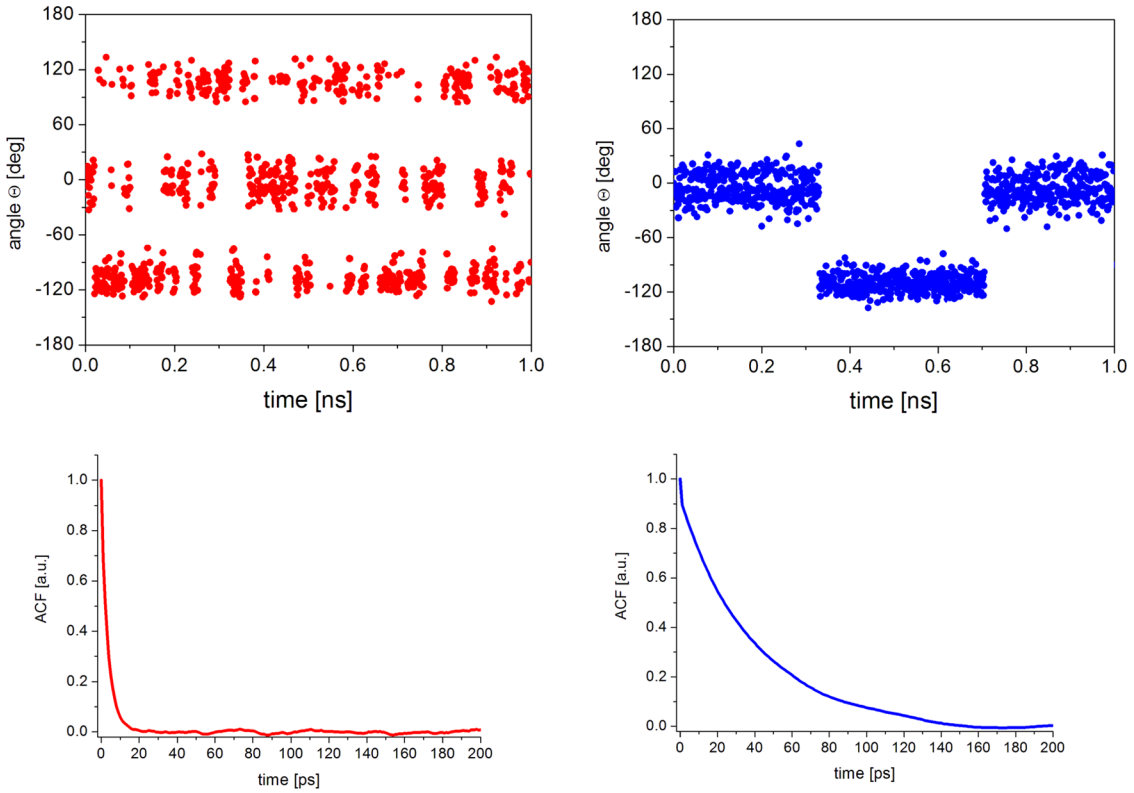

Figure 7. Top: time dependence of the torsional angles $\Theta(t)$ calculated for the methyl groups 4 (left) and 7 (right) belonging to a randomly selected carbimazole molecule. Bottom: angular correlation function corresponding to the reorientation of all of the methyl groups 4 (left) and 7 (right) at 300 K.

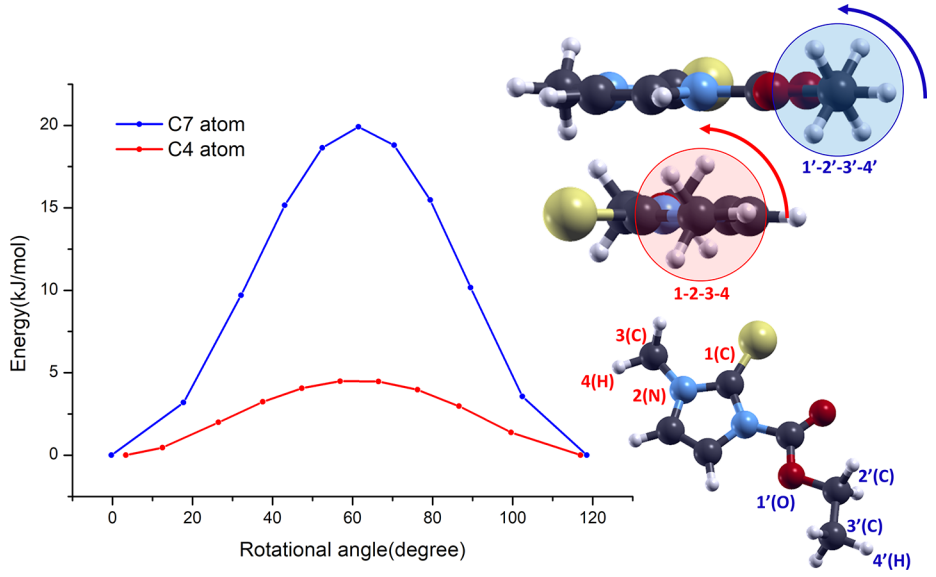

Figure 8. Potential energy surface profiles corresponding to a 120° rotation of the 4 (red, dihedral angle 1−2−3−4) and 7 (blue, dihedral angle 1′−2′−3′−4′) methyl groups around their ternary symmetry axis calculated via NEB algorithm at the DFT level of theory.

First, the time dependence of $\Theta(t)$, defined as the angle swept by the C−H bond vector between $t = 0$ and time t, was analyzed.

Figure 7 shows exemplary $\Theta(t)$ for the two methyl groups 4 and 7. It is clear that both methyl groups exhibit fast small-amplitude librations about a given positions and instantaneous 120° jumps between three well-defined positions. Nevertheless, the frequency of these jumps is quite different for these two methyl groups. The timescale of these reorientational motions can be analyzed through the following angular correlation function (ACF(t))

$$\mathrm{ACF}(t) = \langle \vec{r}_{\mathrm{CH}}(t_0) \cdot \vec{r}_{\mathrm{CH}}(t_0 + t) \rangle \tag{8}$$

where $\vec{r}_{\mathrm{CH}}$ $(t_0 + t)$ is the vector along one C−H bond of a methyl group at time $t_0 + t$ and the brackets indicate an average over all of the methyl groups of the same type in the system and over all possible time origins t_0. By fitting the data of

https://doi.org/10.1021/acs.jpcc.3c00904
J. Phys. Chem. C 2023, 127, 5186−5196

Figure 7 using a single exponential function (ACF(t) ~ exp($-t/\tau_c$)), where τ_c is the correlation time of the reorientational motion, two very different correlation times were found for the two methyl groups: 3.8 and 37 ps for the methyl groups 4 and 7, respectively. The analysis of ACF(t) performed as a function of temperature showed, as expected, that with decreasing temperature, the methyl reorientations slow down following an Arrhenius behavior. The analysis of τ_c vs temperature allowed the obtainment of significantly different activation energies of 4.8 and 18.4 kJ/mol for the methyl groups 4 and 7, respectively.

The estimation of the activation energies was also performed at the DFT level by employing an NEB/DFT approach at zero temperature: the profiles of the PES (potential energy surface) corresponding to the reorientations around the ternary symmetry axis of the C4 and C7 methyl groups are shown in Figure 8 and quantitatively confirm the results achieved at the MD level (see Table 2). To disentangle, at zero temperature, intra and intermolecular effects, the same two rotational barriers have been also calculated at the same level of theory for an isolated carbimazole molecule, finding values of 1.5 and 12.5 kJ/mol for the methyl groups 4 and 7, respectively. The energy barriers for carbimazole in the crystal resulted 4.5 and 19.9 kJ/mol, respectively, indicating that intermolecular interactions strongly influence the values of these barriers. The low value obtained for the methyl group 4 fits the experimental methyl rotation barrier of *N*-methylpyrrole,[49] whereas the value found for the methyl group 7 fits the well-known barrier characterizing the ethane molecule.[50] Interestingly, these estimates are in line with the results of a joint experimental and computational analysis of methyl rotation barriers in organic solids,[51] highlighting two affinities with the present system: (i) the occurrence of both low and medium rotation barriers of methyl groups linked to rigid frameworks and (ii) a quite similar quantitative evolution in the increase of the barriers when passing from isolated molecules to clusters of molecules mimicking crystalline systems. Concerning the latter point, Beckmann[51] in fact found that barriers of the order of 1−2 kJ/mol in an isolated system translate between 2 and 5 kJ/mol in a crystalline environment (as it happens in the present system if we compare the value of the rotation barrier of the methyl group 4), whereas barriers of the order of 8 kJ/mol are characterized by a 1.5-fold increase, resulting in a range around 11−14 kJ/mol (in our case, in agreement with the behavior of the methyl group 7).

DISCUSSION

All of the experimental and computational methods applied in this work show that the sole reorientational motions occurring in crystalline carbimazole are those of the two methyl groups around their ternary symmetry axes. Methyl groups are very important in the molecular recognition of endogenous and exogenous organic compounds by bioreceptors and therefore play a fundamental role in medicinal chemistry. Methyl group reorientations play a unique role, among intramolecular motions, especially because of their low thermal activation, and they have been associated to changes in solubility, binding affinity, and drug metabolism.[18,52,53]

In the case of carbimazole, all of the presented results from QENS, NMR, MD, and DFT confirm that the two methyl reorientations are characterized by very different values of activation energies and correlation times (Table 2 and Figure 9, where the temperature dependence of the correlation times obtained by the different techniques is displayed).

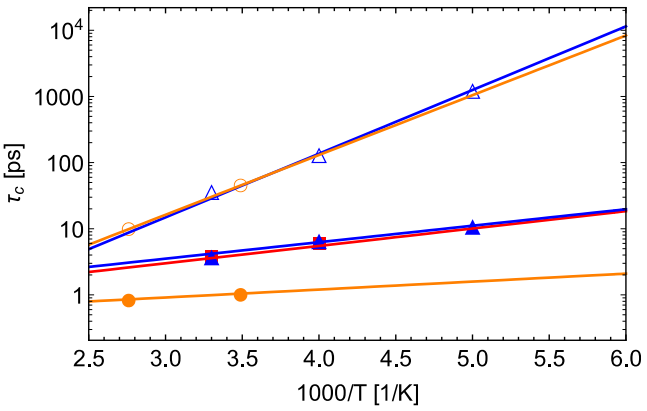

Figure 9. Temperature dependence of the correlation time for methyl reorientation in carbimazole: red square, QENS data; blue triangle solid, blue triangle open, MD simulations; and orange circle solid, orange circle open, NMR data. Closed symbols: methyl group 4, open symbols: methyl group 7. The solid lines are fits of QENS, NMR, and MD data to Arrhenius curves.

In particular, the values obtained by MD and DFT confirm the very different timescale on which the reorientations of the two methyl groups take place, as found by SSNMR. The correlation time and activation energy derived from MD for the reorientation of the methyl group 4 are in good agreement with those obtained by DFT and QENS, while SSNMR gives smaller values. As briefly discussed earlier, this is due to a reorientation too fast to be precisely characterized by SSNMR experiments. On the other hand, the values obtained for the methyl group 7 found from MD and DFT show a perfect agreement with SSNMR results (Table 2 and Figure 9), while this motion is too slow to be revealed by QENS.

The origins of the occurrence of quite different rotation barriers and correlation times for the two methyl groups are not easily identifiable. A first factor to be considered is the steric hindrance, indeed in the ethoxy group, the presence of a CH_2 bonded to the methyl group 7 gives rise to eclipsed conformations that can increase the energy barrier. This is in line with data reported for methyl groups bonded to CH_2 and CH fragments.[43,45,47,54] No other significant differences in steric hindrance are present between the groups 4 and 7, and as already discussed in DFT results, the effect of crystal packing is similar in the two cases.

In addition to conformations and, in general, steric hindrance, electronic effects have been shown to influence methyl rotation barriers. For example, smaller barriers were calculated for *N*-methyl thioamides with respect to *N*-methyl amides.[55] This could be one of the effects influencing the activation energy of methyl 4 in carbimazole. A low activation energy has been reported also for OCH_3 in aspirin[56] and for small molecular crystals such as methyl iodide, methyl bromide, 3-methylthiophene, *p*-xylene, and methyl isocyanate.[57] Low rotational barriers were also recently observed in apilimod and tetrandrine, antiviral drugs proposed for the treatment of SARS-CoV-2.[17]

It is worth noting that differences of correlation times and energy barriers for reorientations of different methyl groups, similar to those observed here by us, have been previously observed in other pharmaceutical compounds like felodipine,[58]

https://doi.org/10.1021/acs.jpcc.3c00904
J. Phys. Chem. C 2023, 127, 5186−5196

nimodipine,[59] and phenacetin;[14] in all of these cases, methyl groups bonded to CH_2 and CH fragments show higher activation energies.

CONCLUSIONS

In this paper, by combining complementary experimental (quasielastic neutron scattering and solid-state nuclear magnetic resonance) and theoretical (molecular dynamics simulations and DFT) methods, the molecular motions of crystalline carbimazole—a drug used in hyperthyroidism treatment—were investigated in detail. The results can be summarized as follows: (i) the reorientation of the ethyl moiety as a whole is frozen in the timescale of our experiments; (ii) the only active internal reorientational motions of carbimazole are those of the two methyl groups (4 and 7); (iii) these two motions are characterized by very different correlation times (differing by almost 2 orders of magnitude at room temperature, the motion of group 4 being much faster) and activation energies (~5 and ~19 kJ/mol for methyl groups 4 and 7, respectively); (iv) the QENS and SSNMR experimental data were confirmed by results predicted by MD simulations and DFT calculations; and (v) the results here obtained are in very good agreement with those reported in the literature for other molecules containing methyl groups in similar chemical environments.

ASSOCIATED CONTENT

Supporting Information

The Supporting Information is available free of charge at https://pubs.acs.org/doi/10.1021/acs.jpcc.3c00904.

Figure S1: FWHM of the Lorentzian functions used to fit to QENS spectra; Table S1: mean square displacement values calculated for individual atoms of the carbimazole molecule at 300 K (PDF)

AUTHOR INFORMATION

Corresponding Authors

Marco Geppi − *Department of Chemistry and Industrial Chemistry, University of Pisa, 56124 Pisa, Italy; Institute for the Chemistry of Organometallic Compound, National Council of Research (ICCOM-CNR), 56124 Pisa, Italy; Center for Instrument Sharing of the University of Pisa (CISUP), 56124 Pisa, Italy;* orcid.org/0000-0002-2422-8400; Email: marco.geppi@unipi.it

Aleksandra Pajzderska − *Faculty of Physics, Adam Mickiewicz University, 61-614 Poznań, Poland;* orcid.org/0000-0002-8096-7718; Email: apajzder@amu.edu.pl

Authors

Andrea Scarperi − *Department of Chemistry and Industrial Chemistry, University of Pisa, 56124 Pisa, Italy*

Elisa Carignani − *Institute for the Chemistry of Organometallic Compound, National Council of Research (ICCOM-CNR), 56124 Pisa, Italy; Center for Instrument Sharing of the University of Pisa (CISUP), 56124 Pisa, Italy;* orcid.org/0000-0001-5848-9660

Francesca Martini − *Department of Chemistry and Industrial Chemistry, University of Pisa, 56124 Pisa, Italy; Center for Instrument Sharing of the University of Pisa (CISUP), 56124 Pisa, Italy*

Jan P. Embs − *Laboratory for Neutron Scattering and Imaging, Paul Scherrer Institut, 5232 Villigen, Switzerland;* orcid.org/0000-0002-2816-2875

Jan Wąsicki − *Faculty of Physics, Adam Mickiewicz University, 61-614 Poznań, Poland;* orcid.org/0000-0002-1586-1191

Giovanni Barcaro − *Institute for Chemical and Physical Processes, National Council of Research (IPCF-CNR), 56124 Pisa, Italy*

Complete contact information is available at: https://pubs.acs.org/10.1021/acs.jpcc.3c00904

Notes

The authors declare no competing financial interest.

ACKNOWLEDGMENTS

This research was partially funded by the University of Pisa, Grant PRA_2020_21. CISUP (Center for Instrument Sharing-University of Pisa) is acknowledged for the use of the Bruker Avance Neo 500 solid-state NMR spectrometer. This research was also supported in part by PLGrid Infrastructure.

REFERENCES

(1) Allen, L. V. Dosage Form Design and Development. *Clin. Ther.* **2008**, *30*, 2102−2111.

(2) Veber, D. F.; Johnson, S. R.; Cheng, H.-Y.; Smith, B. R.; Ward, K. W.; Kopple, K. D. Molecular Properties That Influence the Oral Bioavailability of Drug Candidates. *J. Med. Chem.* **2002**, *45*, 2615−2623.

(3) Aronson, M.; Beckmann, P.; Ross, B.; Tan, S. L. Intramolecular Reorientations and the Effects of Thermal History and Hydrogen Bonding in Four Closely Related Organic Molecular Solids. *Chem. Phys.* **1981**, *63*, 349−358.

(4) Schachter, D. M.; Xiong, J.; Tirol, G. C. Solid State NMR Perspective of Drug−Polymer Solid Solutions: A Model System Based on Poly(Ethylene Oxide). *Int. J. Pharm.* **2004**, *281*, 89−101.

(5) Hodgkinson, P. In *NMR Crystallography*; Harris, R. K., Wasylishen, R. E., Duer, M. J., Eds.; EMR Handbooks, John Wiley & Sons: Chichester, 2009; Chapter Intramolecular Motion in Crystalline Organic Solids, pp. 375−386.

(6) Harris, R. K.; Wasylishen, R. E.; Duer, M. J. *NMR Crystallography*, 1st ed.; John Wiley and Sons, Ltd.: Chichester, U.K., 2009.

(7) Bryce, D. L. NMR Crystallography: Structure and Properties of Materials from Solid-State Nuclear Magnetic Resonance Observables. *IUCrJ* **2017**, *4*, 350−359.

(8) Yee, A. A.; Savchenko, A.; Ignachenko, A.; Lukin, J.; Xu, X.; Skarina, T.; Evdokimova, E.; Liu, C. S.; Semesi, A.; Guido, V.; et al. NMR and X-Ray Crystallography, Complementary Tools in Structural Proteomics of Small Proteins. *J. Am. Chem. Soc.* **2005**, *127*, 16512−16517.

(9) Hodgkinson, P. NMR Crystallography of Molecular Organics. *Prog. Nucl. Magn. Reson. Spectrosc.* **2020**, *118*−*119*, 10−53.

(10) Berendt, R. T.; Sperger, D. M.; Munson, E. J.; Isbester, P. K. Solid-State NMR Spectroscopy in Pharmaceutical Research and Analysis. *TrAC, Trends Anal. Chem.* **2006**, *25*, 977−984.

(11) Harris, R. K. Applications of Solid-State NMR to Pharmaceutical Polymorphism and Related Matters. *J. Pharm. Pharmacol.* **2010**, *59*, 225−239.

(12) Geppi, M.; Mollica, G.; Borsacchi, S.; Veracini, C. A. Solid-State NMR Studies of Pharmaceutical Systems. *Appl. Spectrosc. Rev.* **2008**, *43*, 202−302.

(13) Li, M.; Xu, W.; Su, Y. Solid-State NMR Spectroscopy in Pharmaceutical Sciences. *TrAC, Trends Anal. Chem.* **2021**, *135*, No. 116152.

(14) Bordallo, H. N.; Zakharov, B. A.; Boldyreva, E. V.; Johnson, M. R.; Koza, M. M.; Seydel, T.; Fischer, J. Application of Incoherent Inelastic Neutron Scattering in Pharmaceutical Analysis: Relaxation Dynamics in Phenacetin. *Mol. Pharmaceutics* **2012**, *9*, 2434−2441.
(15) Tsapatsaris, N.; Kolesov, B. A.; Fischer, J.; Boldyreva, E. V.; Daemen, L.; Eckert, J.; Bordallo, H. N. Polymorphism of Paracetamol: A New Understanding of Molecular Flexibility through Local Methyl Dynamics. *Mol. Pharmaceutics* **2014**, *11*, 1032−1041.
(16) Pajzderska, A.; Gonzalez, M. A.; Embs, J. P.; Mielcarek, J.; Wąsicki, J. W. Dynamics of an Amorphous Pharmacologically Active Compound − Diazepam: A QENS Study Combined with Molecular Dynamics Simulations. *RSC Adv.* **2017**, *7*, 35504−35515.
(17) Mamontov, E.; Cheng, Y.; Daemen, L. L.; Kolesnikov, A. I.; Ramirez-Cuesta, A. J.; Ryder, M. R.; Stone, M. B. Low Rotational Barriers for the Most Dynamically Active Methyl Groups in the Proposed Antiviral Drugs for Treatment of SARS-CoV-2, Apilimod and Tetrandrine. *Chem. Phys. Lett.* **2021**, *777*, No. 138727.
(18) Mamontov, E.; Cheng, Y.; Daemen, L. L.; Kolesnikov, A. I.; Ramirez-Cuesta, A. J.; Ryder, M. R.; Stone, M. B. Hydration-Induced Disorder Lowers the Energy Barriers for Methyl Rotation in Drug Molecules. *J. Phys. Chem. Lett.* **2020**, *11*, 10256−10261.
(19) Bée, M. *Quasielastic Neutron Scattering: Principles and Applications in Solid State Chemistry, Biology, and Material Science*, 1st ed.; Hilger, A., Ed.; Taylor & Francis: Bristol, England, 1988.
(20) Müller, K.; Geppi, M. Application of SSNMR to Selected Classes of Systems. In *Solid State NMR: Principles, Methods, and Applications*; Wiley-VCH: Weinheim, Germany, 2021; pp 447−530.
(21) Reif, B.; Ashbrook, S. E.; Emsley, L.; Hong, M. Solid-State NMR Spectroscopy. *Nat. Rev. Methods Primers* **2021**, *1*, No. 1.
(22) Car, R.; Parrinello, M. Unified Approach for Molecular Dynamics and Density-Functional Theory. *Phys. Rev. Lett.* **1985**, *55*, 2471−2474.
(23) Henkelman, G.; Uberuaga, B. P.; Jónsson, H. A Climbing Image Nudged Elastic Band Method for Finding Saddle Points and Minimum Energy Paths. *J. Chem. Phys.* **2000**, *113*, 9901−9904.
(24) Bennett, P. N.; Brown, M. J.; Sharma, P. *Clinical Pharmacology*, 11th ed.; Churchill Livingstone: London, U.K., 2012.
(25) Martini, L. *Encyclopedia of Endocrine Diseases*, 1st ed.; Academic Press, 2004.
(26) Burch, H. B.; Cooper, D. S. Anniversary Review: Antithyroid Drug Therapy: 70 Years Later. *Eur. J. Endocrinol.* **2018**, *179*, R261−R274.
(27) Cooper, D. S. Antithyroid Drugs. *N. Engl. J. Med* **2005**, *352*, 905−917.
(28) Scarperi, A.; Barcaro, G.; Pajzderska, A.; Martini, F.; Carignani, E.; Geppi, M. Structural Refinement of Carbimazole by NMR Crystallography. *Molecules* **2021**, *26*, 4577.
(29) Azuah, R. T.; Kneller, L. R.; Qiu, Y.; Tregenna-Piggott, P. L. W.; Brown, C. M.; Copley, J. R. D.; Dimeo, R. M. DAVE: A Comprehensive Software Suite for the Reduction, Visualization, and Analysis of Low Energy Neutron Spectroscopic Data. *J. Res. Natl. Inst. Stand. Technol.* **2009**, *114*, 341−358.
(30) Richard, D.; Ferrand, M.; Kearley, G. J. Analysis and Visualisation of Neutron-Scattering Data. *J. Neutron Res.* **1996**, *4*, 33−39.
(31) Torchia, D. A. The Measurement of Proton-Enhanced Carbon-13 T_1 Values by a Method Which Suppresses Artifacts. *J. Magn. Reson.* **1978**, *30*, 613−616.
(32) Guan, X.; Stark, R. E. A General Protocol for Temperature Calibration of MAS NMR Probes at Arbitrary Spinning Speeds. *Solid State Nucl. Magn. Reson.* **2010**, *38*, 74−76.
(33) Giannozzi, P.; Baroni, S.; Bonini, N.; Calandra, M.; Car, R.; Cavazzoni, C.; Ceresoli, D.; Chiarotti, G. L.; Cococcioni, M.; Dabo, I.; et al. QUANTUM ESPRESSO: A Modular and Open-Source Software Project for Quantum Simulations of Materials. *J. Phys.: Condens. Matter* **2009**, *21*, No. 395502.
(34) Blöchl, P. E. Projector Augmented-Wave Method. *Phys. Rev. B* **1994**, *50*, 17953−17979.
(35) Perdew, J. P.; Burke, K.; Ernzerhof, M. Generalized Gradient Approximation Made Simple. *Phys. Rev. Lett.* **1996**, *77*, 3865−3868.
(36) Grimme, S. Semiempirical GGA-Type Density Functional Constructed with a Long-Range Dispersion Correction. *J. Comput. Chem.* **2006**, *27*, 1787−1799.
(37) Das, D.; Roy, G.; Mugesh, G. Antithyroid Drug Carbimazole and Its Analogues: Synthesis and Inhibition of Peroxidase-Catalyzed Iodination of L-Tyrosine. *J. Med. Chem.* **2008**, *51*, 7313−7317.
(38) Todorov, I. T.; Smith, W.; Trachenko, K.; Dove, M. T. DL_POLY_3: New Dimensions in Molecular Dynamics Simulations via Massive Parallelism. *J. Mater. Chem.* **2006**, *16*, 1911−1918.
(39) Berendsen, H. J. C.; Postma, J. P. M.; van Gunsteren, W. F.; DiNola, A.; Haak, J. R. Molecular Dynamics with Coupling to an External Bath. *J. Chem. Phys.* **1984**, *81*, 3684−3690.
(40) Hinsen, K.; Pellegrini, E.; Stachura, S.; Kneller, G. R. nMoldyn 3: Using Task Farming for a Parallel Spectroscopy-Oriented Analysis of Molecular Dynamics Simulations. *J. Comput. Chem.* **2012**, *33*, 2043−2048.
(41) Forte, C.; Geppi, M.; Malvaldi, M.; Mattoli, V. Dynamics of an Amorphous Polymer by an Improved NMR Approach Based on the Simultaneous Analysis of ^{1}H and ^{13}C Relaxation Times. *J. Phys. Chem. B* **2004**, *108*, 10832−10837.
(42) Carignani, E.; Borsacchi, S.; Geppi, M. Detailed Characterization of the Dynamics of Ibuprofen in the Solid State by a Multi-Technique NMR Approach. *ChemPhysChem* **2011**, *12*, 974−981.
(43) Carignani, E.; Borsacchi, S.; Geppi, M. Dynamics by Solid-State NMR: Detailed Study of Ibuprofen Na Salt and Comparison with Ibuprofen. *J. Phys. Chem. A* **2011**, *115*, 8783−8790.
(44) Mollica, G.; Forte, C.; Malvaldi, M.; Geppi, M. Dynamics of Ethylene−Propylene Random Copolymers by 1H and 13C Solid-State NMR. *J. Phys. Chem. B* **2011**, *115*, 1978−1985.
(45) Carignani, E.; Borsacchi, S.; Blasi, P.; Schoubben, A.; Geppi, M. Dynamics of Clay-Intercalated Ibuprofen Studied by Solid State Nuclear Magnetic Resonance. *Mol. Pharmaceutics* **2019**, *16*, 2569−2578.
(46) Delage, C.; Faure, F.; Leger, J. M.; Raby, C.; Goursolle, M. Conformational Study of 3-Methyl 2-Thio Imidazoline Ethyl 1-Carboxylate. *C. R. Acad. Sci.* **1990**, *311*, 781−784.
(47) Apperley, D. C.; Markwell, A. F.; Frantsuzov, I.; Ilott, A. J.; Harris, R. K.; Hodgkinson, P. NMR Characterisation of Dynamics in Solvates and Desolvates of Formoterol Fumarate. *Phys. Chem. Chem. Phys.* **2013**, *15*, 6422−6430.
(48) Torchia, D. A.; Szaba, A. Spin-Lattice relaxation in Solids. *J. Magn. Reson.* **1982**, *49*, 107−121.
(49) Van, V.; Stahl, W.; Nguyen, H. V. L. Two Equivalent Methyl Internal Rotations in 2,5-Dimethylthiophene Investigated by Microwave Spectroscopy. *Phys. Chem. Chem. Phys.* **2015**, *17*, 32111−32114.
(50) Kemp, J. D.; Pitzer, K. S. Hindered Rotation of the Methyl Groups in Ethane. *J. Chem. Phys.* **1936**, *4*, 749.
(51) Beckmann, P. A.; Conn, K. G.; Mallory, C. W.; Mallory, F. B.; Rheingold, A. L.; Rotkina, L.; Wang, X. Distributions of Methyl Group Rotational Barriers in Polycrystalline Organic Solids. *J. Chem. Phys.* **2013**, *139*, No. 204501.
(52) Nickels, J. D.; Curtis, J. E.; O'Neill, H.; Sokolov, A. P. Role of Methyl Groups in Dynamics and Evolution of Biomolecules. *J. Biol. Phys.* **2012**, *38*, 497−505.
(53) Barreiro, E. J.; Kümmerle, A. E.; Fraga, C. A. M. The Methylation Effect in Medicinal Chemistry. *Chem. Rev.* **2011**, *111*, 5215−5246.
(54) Martini, F.; Borsacchi, S.; Spera, S.; Carbonera, C.; Cominetti, A.; Geppi, M. P3HT/PCBM Photoactive Materials for Solar Cells: Morphology and Dynamics by Means of Solid-State NMR. *J. Phys. Chem. C* **2013**, *117*, 131−139.
(55) Wiberg, K. B.; Rush, D. J. Methyl Rotational Barriers in Amides and Thioamides. *J. Org. Chem.* **2002**, *67*, 826−830.
(56) Kitchin, S. J.; Halstead, T. K. Solid-State ^{2}H NMR Studies of Methyl Group Dynamics in Aspirin and Aspirin · β-Cyclodextrin. *Appl. Magn. Reson.* **1999**, *17*, 283−300.

https://doi.org/10.1021/acs.jpcc.3c00904
J. Phys. Chem. C 2023, 127, 5186−5196

(57) Langen, H.; Montjoie, A.-S.; Müller-Warmuth, W.; Stiller, H. NMR T_1-Analysis of Methyl Tunnelling in Molecular Crystals at Intermediate Barriers. *Z. Naturforsch. A* **1987**, *42*, 1266−1274.
(58) Pajzderska, A.; Drużbicki, K.; Gonzalez, M. A.; Jenczyk, J.; Mielcarek, J.; Wąsicki, J. Diversity of Methyl Group Dynamics in Felodipine: A DFT Supported NMR and QENS Study. *CrystEngComm* **2018**, *20*, 7371−7385.
(59) Drużbicki, K.; Pajzderska, A.; Kiwilsza, A.; Jenczyk, J.; Chudoba, D.; Jarek, M.; Mielcarek, J.; Wąsicki, J. In Search of the Mutual Relationship between the Structure, Solid-State Spectroscopy and Molecular Dynamics in Selected Calcium Channel Blockers. *Eur. J. Pharm. Sci.* **2016**, *85*, 68−83.

https://doi.org/10.1021/acs.jpcc.3c00904
J. Phys. Chem. C 2023, 127, 5186−5196